

Electronic Supplementary Information of

Au Nanoparticles Decorated Reduced Graphene Oxide and its Electroanalytical Characterization for Label Free Dopamine Detection

C. Ingrosso,^{a,b} M. Corricelli,^c A. Testolin,^d V. Pifferi,^d F. Bettazzi,^e G. V. Bianco,^f N. Depalo,^a E.

Fanizza,^{a,b,c} M. Striccoli,^a I. Palchetti,^{b,e,} M. L. Curri^{a,b,c,*}, L. Falciola^{b,d,*}*

^aCNR-IPCF S.S. Bari, c/o Dept. of Chemistry, Università degli Studi di Bari, via Orabona 4, I-70126 Bari, Italy.

^bConsorzio Interuniversitario Nazionale per la Scienza e Tecnologia dei Materiali (INSTM), Via G. Giusti, 9 50121 Firenze (Italy)

^cDept. of Chemistry, Università degli Studi di Bari, via Orabona 4, I-70126 Bari, Italy.

^dDept. of Chemistry, Università degli Studi di Milano, via Golgi 19, 20133, Milano, Italy.

^eDept. of Chemistry Ugo Schiff, Università degli Studi di Firenze, via della Lastruccia 3-13, 50019 Sesto Fiorentino (Fi), Italy.

^fCNR-NANOTEC Sez. Bari, c/o Dept. of Chemistry, Università degli Studi di Bari, Via Orabona 4, I-70126 Bari, Italy.

*Email: marialucia.curri@uniba.it, luigi.falciola@unimi.it, ilaria.palchetti@unifi.it

Fig. S1 shows TEM images of the nanostructures achieved in the two preliminary control experiments, performed by synthesizing the Au NPs onto AP-RGO flakes in 1-octadecene (ODE) and in absence of OLEAM, and onto bare RGO sheets in OLEAM.

The nanostructures achieved in the first control experiment show high contrast, 100-250 nm sized Au nanostructures, multifaceted and partially aggregated onto the RGO basal plane, that form by

spontaneous galvanic reduction processes induced by electron transfers from RGO to $\text{HAuCl}_4 \times 3\text{H}_2\text{O}$ (Fig. S1(A)).¹ When the Au NPs were synthesized onto bare RGO sheets in OLEAM, the TEM micrographs show only few and small high contrast nano-objects heteronucleated onto the RGO sheets (Fig. S1(B)), that are ascribed to Au NPs formed by galvanic reduction,¹ and nearly spherical high image contrast nanostructures, 9.6 ± 2.7 nm in size, likely ascribed to homonucleated Au NPs (Fig. S1(C)).

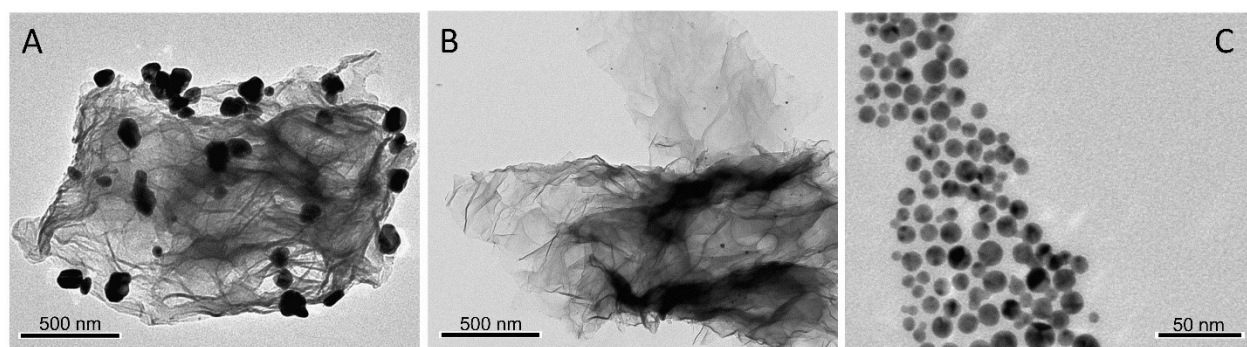


Fig. S1 TEM images of the (A) AP-RGO/Au NPs synthesized with the 1:340 AP-RGO: $\text{HAuCl}_4 \times 3\text{H}_2\text{O}$ w/w in ODE and in absence of OLEAM, (B) hybrid pellet isolated and (C) supernatant collected by centrifugation from the dispersion of the Au NPs synthesized, *in situ*, onto bare RGO.

Fig S2 reports the TEM image of the AP-RGO/Au NPs hybrid nanocomposite, as-synthesized and isolated by centrifugation.

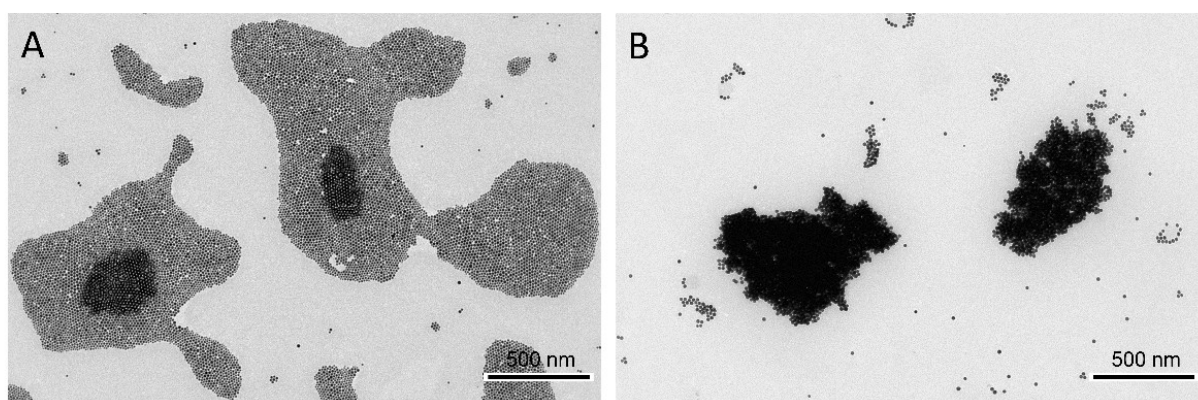


Fig. S2 TEM images of the AP-RGO/Au NPs sample synthesized with the 12:1 OLEAM:HAuCl₄ × 3H₂O molar ratio at the 1:340 AP-RGO:HAuCl₄ × 3H₂O w/w, (A) before and (B) after isolation by centrifugation.

Fig. S3 reports the UV-Vis absorption and TEM image of the OLEAM-Au NPs.

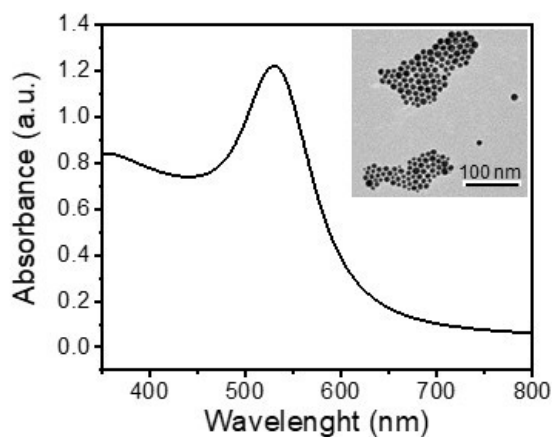


Fig. S3 UV-Vis absorption spectrum of a 1:120 diluted OLEAM-Au NPs toluene solution synthesized from 0.17 M Au precursor. (In the inset) TEM image of OLEAM-Au NPs.

Fig. S4 reports the CVs and Bode plots recorded at the SPCEs modified by AP-RGO, OLEAM-Au NPs and at the A_OLEAM electrode, in 0.1 M PBS buffer (pH = 7.4) added by 3 mM K₄[Fe(CN)₆].

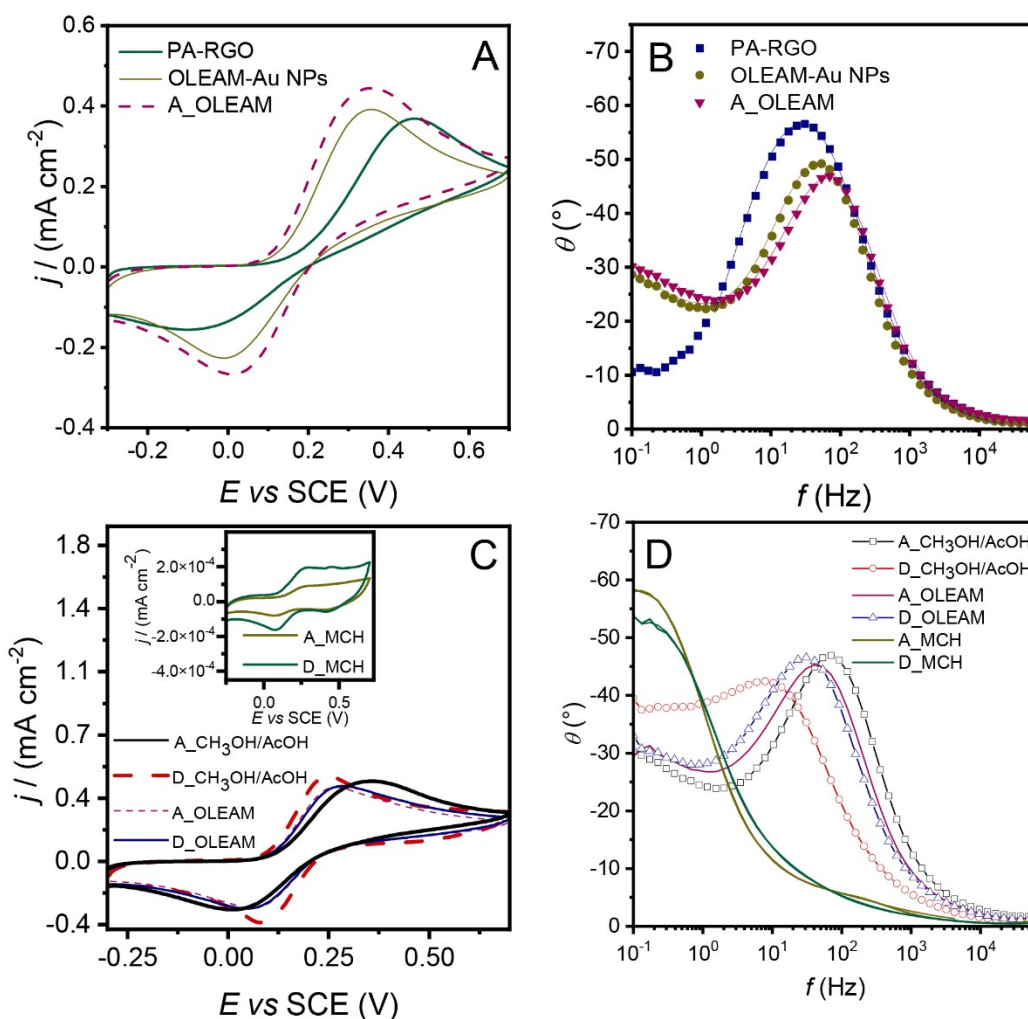


Fig. S4 (A) CVs at the scan rate of 0.1 V s^{-1} and step potential of 0.005 V , between -0.3 V - 0.7 V , and (B) Bode plots at $+0.25 \text{ V}$ in 0.1 M PBS added by $3 \text{ mM K}_4[\text{Fe}(\text{CN})_6]$, of AP-RGO, OLEAM-Au NPs and A_OLEAM. (C) CVs and (D) Bode plots of A_OLEAM, D_OLEAM, A_CH₃OH/AcOH, D_CH₃OH/AcOH and A_MCH and D_MCH, at $+0.25 \text{ V}$ in 0.1 M PBS ($\text{pH}= 7.4$) added by $3 \text{ mM K}_4[\text{Fe}(\text{CN})_6]$.

For all the investigated electrodes, the figure shows the quasi-reversible redox peaks typical of $[\text{Fe}(\text{CN})_6]^{3-/4-}$ along with a decrease of ΔE_p and an increase of the current density, passing from SPCEs modified by AP-RGO to those based on OLEAM-Au NPs and to A_OLEAM electrodes (Fig. S5(A)). This evidence agrees with the results of Fig. 6, attesting for the enhancement of the electroactive surface area, electrode conductivity and heterogeneous charge transfer capability at the

electrode/electrolyte interface of the hybrid modified SPCEs, with respect to the OLEAM-coated Au NPs and AP-RGO.

The Bode plot confirms the results obtained by CV showing higher frequencies for the Au based samples, explained by an easier and faster charge transfer between the probe molecule and the electrode, enhanced for A_OLEAM.

In agreement to what observed in Fig. 6, also in presence of the redox probe, the CVs of the A_OLEAM and D_OLEAM exhibit almost the same peak potentials and the same currents due to the presence of the OLEAM insulating ligand molecule coordinated to the Au NPs surface, acting as barrier to the charge transfers. For the same reason, the Bode plots of the A_OLEAM and D_OLEAM show very similar frequencies. After spin-coating CH₃OH/AcOH, both samples show the increase of the peak current indicating the displacement of OLEAM (Fig. S4(C)-(D)). After removal of OLEAM, A_CH₃OH/AcOH moves to higher frequencies showing a faster and easier charge transfer, whereas D_CH₃OH/AcOH moves to lower frequencies.

When the electrodes were treated by incubation in MCH (inset of Fig. S4(C)) they show almost the same behavior observed in the inset of Fig. 6(C). The current presents a capacitive behavior and the currents increase showing two reduction peaks at ca. +0.088 and +0.41 V. The only difference in presence of the K₄[Fe(CN)₆] probe is that the anodic current tends to a step-like line-shape, and that two oxidation shoulders are evident at +0.3 V and +0.4 V (inset of Fig. S4(C)).

The Bode plots of the A_MCH and D_MCH electrodes (Fig. S4(D)) show the same evidence as the plots of fig. 6(D), meaning that, probably, due to the capacitive behavior, the charge transfer between the probe and the electrode is very low and difficult.

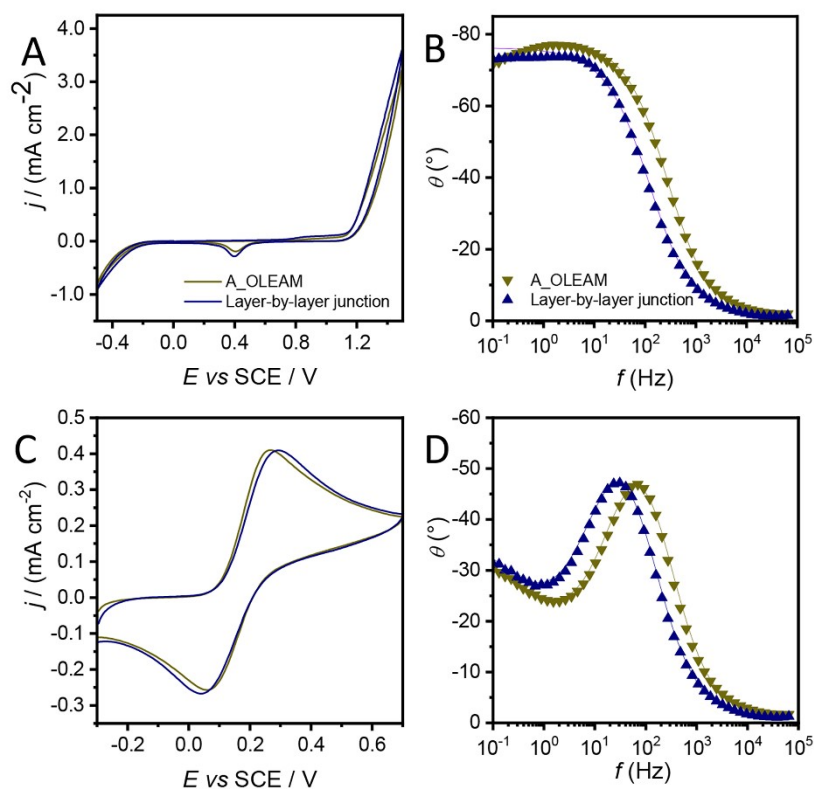


Fig. S5 (A-C) CVs and (B-D) Bode plots at +0.25 V of A_OLEAM and layer-by-layer junction. The CVs and Bode plots are recorded in 0.1 M PBS (A-B) as neat and added by 3mM $K_4[Fe(CN)_6]$ in (C-D).

The CVs recorded in neat PBS buffer (fig. S5(A)) show that the electrochemical activity of the OLEAM-Au NPs is very similar to those of the A_OLEAM and layer-by-layer junction modified electrodes. Conversely, the Bode plots of Fig. S5(B) show a deviation from the pure-capacitor behavior in the layer-by-layer junction at lower frequencies, reasonably explained by the lack of the PA linker between Au NPs and the RGO sheets.

Moreover, in presence of $K_4[Fe(CN)_6]$, A_OLEAM shows a decrease of ΔE_p (Fig. S5(C)) and a faster and easier charge transfer (Fig. S5(D)) confirming the essential role of PA in favoring the charge transfer between the hybrid components, and hence, in improving the electrochemical activity of the hybrid nanocomposite electrodes.

Table S1: Estimated LODs of electrodes modified by graphene based nanocomposites applied for the detection of DA.

Electrode	Linearity range (μM)	LOD (μM)	Ref
RGO and Au NPs	0.02-200.00	0.0150	2
Bi_2S_3 nanorods-RGO nanocomposites	0.01-40.00	0.0120	3
AuPt NPs on Sulfonated N/S co-doped Graphene	0.01-50.00	0.0060	4
3D RGO/AuPd NPs	0.50-135.00	0.2000	5
AuNPs@GO/PPy/Carbon Fiber Paper	---	0.1150	6
PA-RGO/Au NPs	0.013-0.130	0.0025	This work

Fig. S6 reports the calibration curves of A_OLEAM and A_CH₃OH/AcOH, recorded by amperometry at +0.70 V at increasing concentrations of H₂O₂. As it can be noticed, irrespectively of the treatment of the A_OLEAM electrodes, the current density increases upon successive additions of H₂O₂, but the treatment with methanol and acetic acid decreases the current density response of the hybrid modified electrode.

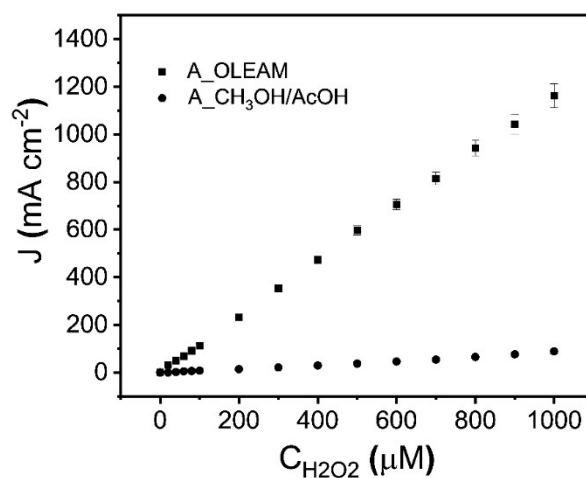


Fig. S6 Amperometric response of H₂O₂ at A_OLEAM and A_CH₃OH/AcOH, in 0.05 M PBS (pH 8.0) at + 0.70 V (SCE), under stirring condition.

References

1. L. Magagnin, R. Maboudian, C. Carraro, *J. Phys. Chem. B* 2002, **106**, 401.
2. X. Huang, W. Shi, N. Bao, C. Yu, H. Gu, *Microchim. Acta* 2019, **186**, 310.

3. C. Tan, J. Zhao, P. Sun, W. Zheng, G. Cui, *New J. Chem.* 2020, **44**, 4916.
4. J. Gu, Q. An, J. Chen, Y. He and W. Huang, *Inorg. Chem. Commun.*, 2023, **147**, 110282.
5. X. Yan, Y. Gu, C. Li, B. Zheng, Y. Li, T. Zhang, Z. Zhang and M. Yang, *Sensor. Actuat. B - Chem.*, 2018, **257**, 936.
6. K. Zhang, X. Chen, Z. Li, Y. Wang, S. Sun, L. Wang, T. Guo, D. Zhang, Z. Xue, X. Zhou and X. Lu, *Talanta*, 2018, **178**, 315.
7. Y. Hou, K. Sheng, Y. Lu, C. Ma, W. Liu, X. Men, L. Xu, S. Yin, B. Dong, X. Bai and H. Song, *Microchim. Acta*, 2018, **185**, 1.